The Thermal Response of a Human in the Near-Zone of a Resonant Thin-Wire Antenna

RONALD J. SPIEGEL, MEMBER, IEEE

Abstract—**The thermal response of a human in the near-zone of an antenna was determined by numerical procedures. The approach taken was to modify the heat transfer equations for man in air to account for thermal loading due to the energy absorbed from the radiating antenna. The absorbed power density distribution in the human body was determined by considering the body and antenna to be a coupled system in which the resulting system of equations were solved by moment method procedures. This information was then analyzed by a thermal response model consisting of a series of transient conduction equations with internal heat generation due to metabolism, internal convective heat transfer due to blood flow, external interaction by convection and radiation, and cooling of the skin by sweating and evaporation. Internal heating patterns were calculated for two cases: a human in the near-zone of a quarter-wave monopole and a half-wave dipole operating at 45 and 200 MHz, respectively. It was found that negligible heating occurred for antennas with input power levels of less than 50 W.**

I. Introduction

THE GENERAL PUBLIC health implications of the electromagnetic (EM) fields emitted by portable/mobile (CB) antennas and by amateur radio antennas are not known. While the greatest majority of experimental results in the area of EM effects in biological systems tend to imply that most of the observed effects are thermal in nature [1], some recent research [2] indicates effects that appear to be nonthermally produced. In order to quantify hazardous EM near-zone field levels via thermal considerations, this research considers the thermal response of a human in close proximity to a radiating antenna.

Thermally harmful effects can occur if the total power absorbed by the body is large enough to cause protective mechanisms for heat control to break down, resulting in an uncontrolled rise in body temperature (hyperthermia). Localized temperature effects, without a significant increase in whole-body temperature, can also occur. Localized temperatures above 41.6°C can cause protein denaturation, coagulation of protein, increased permeability of cell membranes, or the liberation of toxins in the immediate vicinity where the "hot spot" exists. Of course, the severity of the physiologic effects produced by localized temperature increases can be expected to be greatly enhanced in critical organs such as the brain or heart. Thus, it is imperative to be able to quantify the absorption of EM energy into the biosystem and the resulting thermal response if one is to determine if the EM fields emitted by a radiating device are harmful.

There is virtually no quantitative information in regard to the heating patterns in a human subjected to near-zone antenna fields. For ethical reasons this information cannot be acquired using actual human subjects. Therefore, the thermal response of humans from exposure to EM fields can only be achieved by the application of highly sophisticated and realistic numerical models. Although there exist reasonably realistic near-zone EM [3], [4] and heat transfer [5] models for the human body, there has been no reported combination of the two models. To that end, the near-zone EM and heat transfer models were joined in a manner previously utilized for far-zone exposure conditions [5]. The approach taken was to modify the heat transfer equations for man in air to account for thermal loading due to the EM energy absorbed from the antenna. The absorbed power density distribution in the body was determined by considering the antenna and body to be a coupled system in which the resulting integral equations were solved by moment method procedures. This information was then analyzed by a finite element solution to the transient conduction heat-transfer equation which included the effects of internal heat generation due to metabolism, internal convective heat transfer due to blood flow, external interaction with the air by convection and radiation, and cooling of the skin by sweating and evaporation.

Numerical results are presented for the following two cases: a human standing on a ground plane in the near-zone of a $\lambda/4$ monopole operating at 45 MHz, and a human in free-space in which a $\lambda/2$ dipole operating at a frequency of 200 MHz is placed very close to the head. The 45-MHz frequency represents the resonant frequency [6] for a human adult over a ground plane, and the 200-MHz case is relatively close to the resonant frequency (around 375 MHz) of the head [7].

II. Electromagnetic Model

Using the so-called tensor integral method, the complete mathematical description of a thin-wire antenna in close proximity to a biological body has been described elsewhere [3]. Therefore, only a brief summary of the necessary

Manuscript received July 28, 1981; revised September 29, 1981.

The author is with the Bioengineering Branch, Experimental Biology Division, U.S. Environmental Protection Agency, Health Effects Research Laboratory, Research Triangle Park, NC 27711.

equations and their solutions are provided here; readers interested in more detail should consult [3]. From Maxwell's equations, it is straightforward to show that the coupled integral equations necessary to determine both the antenna current distribution and the electric field within the body are given by

$$\left\{1+\frac{\tau(\vec{r})}{3j\epsilon_0\omega}\right\}\vec{E}(\vec{r})-PV\int_{V_b}\tau(\vec{r}')\vec{E}(\vec{r}')\cdot\overleftrightarrow{G}(\vec{r},\vec{r}')\,dV'=\int_{\text{ant}}I(s')\hat{s}'\cdot\overleftrightarrow{G}(\vec{r},s')\,ds' \quad (1)$$

and

$$\hat{s}\cdot\int_{\text{ant}}I(s')\hat{s}'\cdot\overleftrightarrow{G}(s,s')\,ds'+\hat{s}\cdot\int_{V_b}\tau(\vec{r}')\vec{E}(\vec{r}')\cdot\overleftrightarrow{G}(s,\vec{r}')\,dV'=-V_0\delta(s) \quad (2)$$

where

$\vec{E}$	electric field within the body;
I	antenna current;
$\vec{r}$	field point;
$\vec{r'}$	source point interior to the biological body, V_b;
$\overleftrightarrow{G}$	free-space tensor Green's function;
$\hat{s}$	unit vector tangential to the antenna's surface;
$\tau(\vec{r})=\sigma(\vec{r})+j\omega\{\epsilon(\vec{r})-\epsilon_0\}$	complex conductivity;
V	antenna driving point input voltage; and
δ	Dirac delta function.

The other quantities are well known, except possibly the symbol PV which denotes the principal value of the integral (at the point $\vec{r}=\vec{r}'$ the integrand is singular, and the integration is carried out by excluding this point by surrounding it with an infinitesimally small spherical volume).

The solutions for the induced electric field in the body and antenna current are achieved by using Hallen's analysis for the antenna current and using the method of moments to solve the resulting coupled equations. The method of moments solution consists of partitioning the antenna into a number of small segments and dividing the object into a large number of cubical subvolumes and utilizing pulse expansion functions and delta testing functions. This is the well-known point-matching method. The coupled integral equations (1) and (2) can then be approximated by a linear system of equations, which can be symbolically written in matrix form as

$$\begin{bmatrix}[G_{II}] & [G_{IE}]\\ [G_{EI}] & [G_{EE}]\end{bmatrix}\begin{bmatrix}[I]\\ [E]\end{bmatrix}=\begin{bmatrix}[V]\\ [0]\end{bmatrix} \quad (3)$$

where the elements of each submatrix are described elsewhere [8]. In (3), the interaction of the biological body with the antenna is given by the terms with the subscripts IE or EI. The self or noninteracting components are denoted by the subscript II for the antenna and EE for the body. Of course, if the object is far enough from the antenna, then both the $[G_{IE}]$ and $[G_{EI}]$ terms would be essentially equal to zero, i.e., no coupling would occur.

A. $\lambda/4$ Monopole

Fig. 1 illustrates the first situation considered: a human in close proximity to a monopole of height equal to that of the human ($h=1.75$ m). The frequency of the source is 45 MHz, so that the monopole's height is approximately equal to $\lambda/4$. This frequency is close to the body's resonant frequency when located over an infinite ground plane [6]. A block model for a 70-kg man comprised of 180 cubical cells of various sizes was utilized [9]. For the analysis contained here, it is assumed that each cell is composed of tissue that has a relative permittivity value 2/3 times that of muscle. The two-thirds factor is based on average dielectric values for the various body tissues. There is, of course, no inherent restriction in the analysis to homogeneous isotropic dielectric properties for the tissue.

First, consider the fields produced by the antenna at the position of the object. Fig. 2 shows the magnitude of the total electric field $\vec{E}$ versus vertical height from the antenna's base. This curve represents the antenna electric field distribution in the E-plane ($X-Z$ plane) of the antenna at a separation distance of 20 cm. Input power to the antenna is 1 W. Also superimposed on the curve are the orthogonal components (E_x and E_z) of the electric field as denoted by the set of vectors at various positions on the graph. Note that in the E-plane, the third component (E_y) is equal to zero. This vector information is useful because it indicates how well the energy produced by the antenna might be absorbed by the body. For example, it is seen from Fig. 2 that the largest field components produced by the antenna are not generally in the proper direction for maximum absorption by the body. (Maximum absorption occurs when the component parallel to the major length of the body is large.) Thus, it may be anticipated that the antenna will produce a much lower specific absorption rate (SAR) than a plane-wave field in which the electric field vector is oriented parallel to the major length of the body (so-called E-field coupling).

Fig. 3 shows how the electric field falls off with increasing distance from the antenna at a height of 0.8 m. It is seen that the horizontal (E_z) component dominates out to distances of around 1 m ($r/\lambda=0.15$). At distances past that point, the field begins to approach a far-zone field with a characteristic roll-off of $1/R$ with an electric field vector (E_x) oriented primarily in the vertical direction. Thus, with the object placed approximately 20 cm from the antenna, it is clear that it is well within the near-zone of the antenna.

Another consideration is the closeness of the coupling between the antenna and body. This can be ascertained by a consideration of the antenna current. The effect of the body on the antenna current distribution is illustrated in Fig. 4 for an approximately 20-cm separation between the antenna and body. In the figure, the solid line denotes the normalized antenna current distribution in the absence of the body, while the dotted curve shows the antenna current

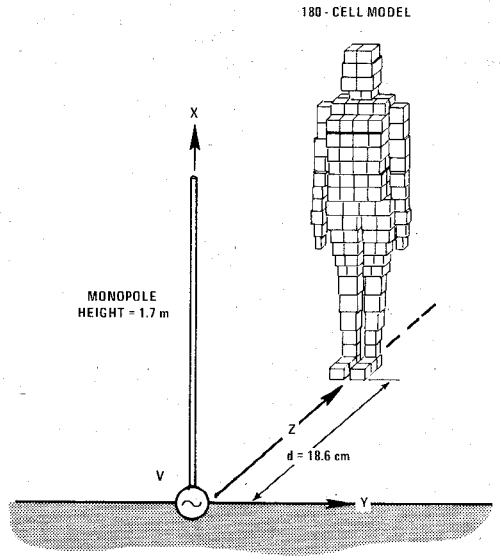

Fig. 1. A $\lambda/4$ monopole antenna in close proximity to the 180-block model of man.

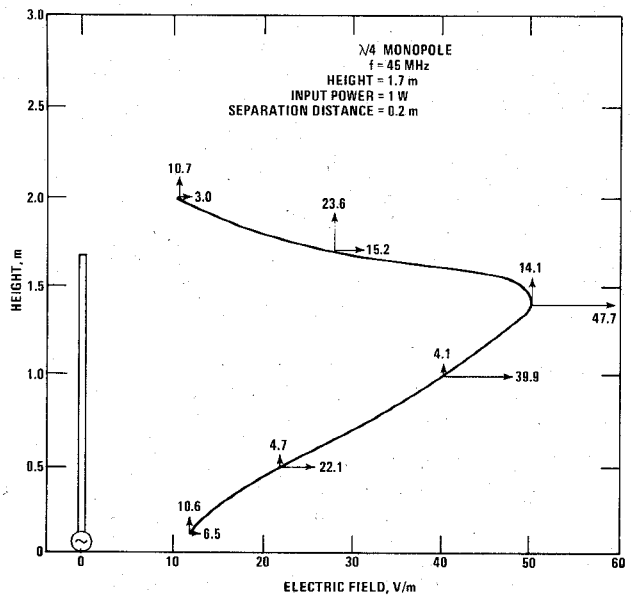

Fig. 2. The near-zone electric field distribution of the $\lambda/4$ monopole antenna at a distance of 20 cm from the antenna.

with the body present. It is seen that the antenna current gets perturbed very little from the free-space situation. As the object is placed closer to the antenna, it is reasonable to assume that the perturbation of the antenna current, and consequently the fields produced by the antenna, will become more significant.

Fig. 5 shows a plot of the absorbed energy density, in watts per cubic meter, through a 1.75-m high human weighing 70 kg, when the body has been irradiated by fields produced from the $\lambda/4$ monopole with an input power of 1 W. As stated earlier, the body is approximately 20 cm from the antenna. Although the power density was calculated for each of the 180 cells, the curve of Fig. 5 represents the average power density in each layer as determined by adding the power density of the individual cells in each layer and dividing that value by the total number of cells in

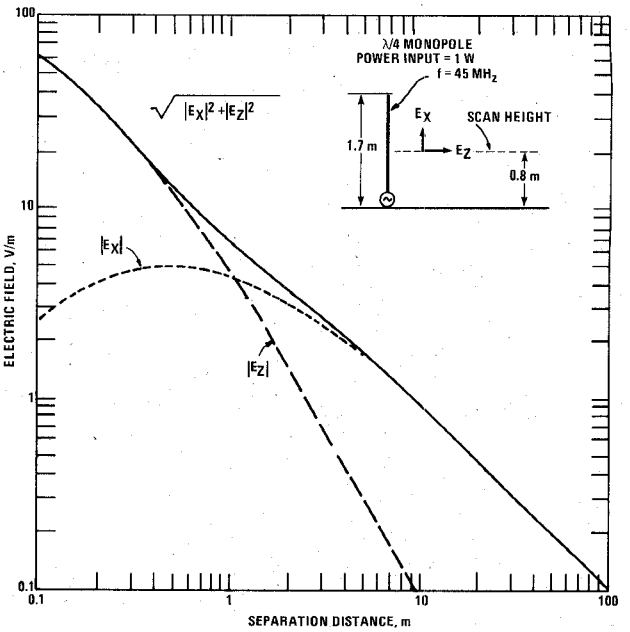

Fig. 3. The near-and far-zone electric field distribution of the $\lambda/4$ monopole antenna as a function of distance from the antenna.

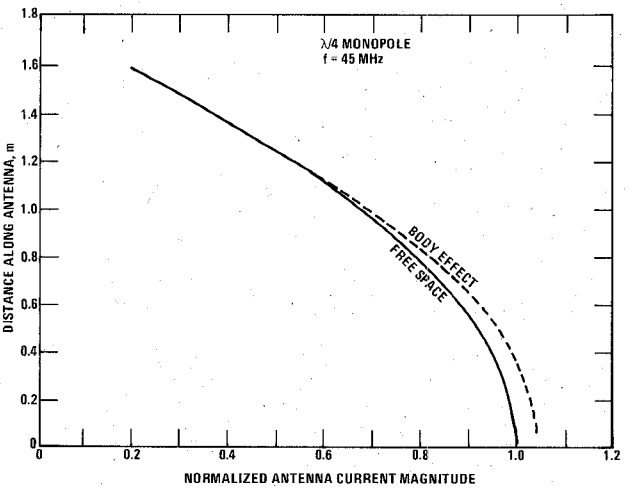

Fig. 4. The EM coupling effect of the body on the antenna current distribution.

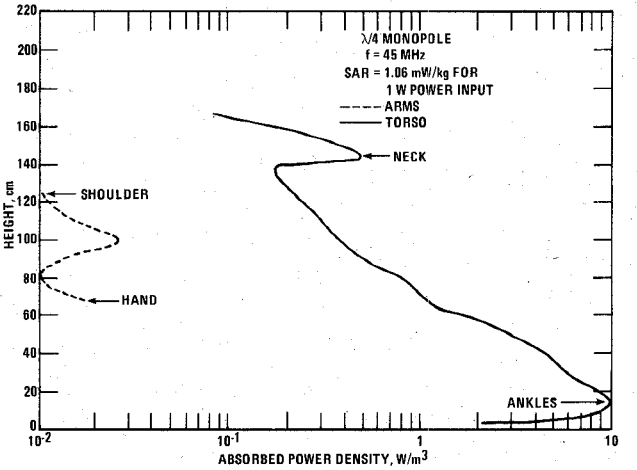

Fig. 5. The absorbed power density inside a human exposed to EM near-zone fields produced by the $\lambda/4$ monopole antenna.

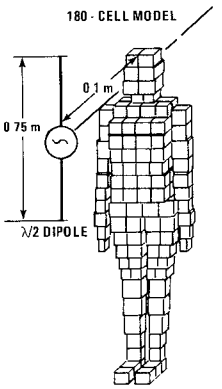

Fig. 6. A $\lambda/2$ dipole antenna in close proximity to the head of the 180-block model of man.

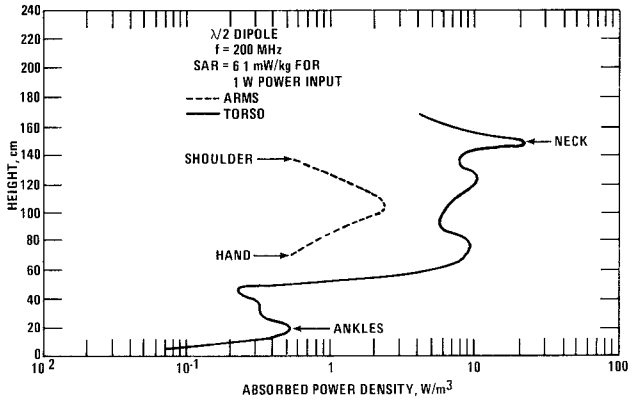

Fig. 7. The absorbed power density inside a human exposed to EM near-zone fields produced by the $\lambda/2$ dipole antenna.

the layer. The area of maximum absorption occurs in the ankles. This is a result of large current densities in the ankles created by currents flowing to ground through the narrow cross-sectional area of the ankles. The arms do not absorb much energy from the field because they are parallel to the large cross-sectional torso which effectively shunts most of the induced currents away from the arms. The total energy absorbed by the body was found to be 74 mW (average whole body SAR = 1.06 mW/kg).

B. $\lambda/2$ Dipole

Next, the case of a $\lambda/2$ dipole operating at a frequency of 200 MHz and placed very close to the head of a human in free-space is considered. Fig. 6 depicts the situation. This frequency was chosen because it is fairly close to the predicted resonant frequency of the head and, in addition, does not violate high frequency limitations of the numerical method [9]. The antenna current distribution and near-field pattern are not significantly different from those of the previous case, so for the sake of brevity plots of these quantities are not given. On the other hand, the absorbed power density distribution for this situation is quite different. As shown in Fig. 7, maximum absorption occurs in the neck. Because the object is located in free-space, the current density falls to zero in the feet and, as a consequence, there is much less power absorbed in the knees than what occurred in the previous situation. In addition, the average whole body SAR of 6.1 mW/kg for 1 W of input power to the antenna is around six times larger than that obtained for the monopole case. As before, the torso tends to shunt most of the induced current density past the arms, so there is smaller absorbed power density levels in the arms than typically are induced in the torso.

III. Heat Transfer Model

The calculated power densities induced in the human model of the previous section are now used as input data to the heat transfer model. The approach taken was to modify the heat transfer equations for a resting man in a thermally neutral environment (temperature = 30°C and relative humidity = 30 percent) to account for the thermal loading due to the energy absorbed from the radiating antenna. The model used here has been described elsewhere [5], so only a brief discussion is presented.

Basically, the heat transfer model is an adaptation of an earlier model [10] for a nude man exposed to an air environment. The primary modification to this model consisted of dividing the object up into a finer number of finite elements in which heat transfer can occur not only from the core to the skin, but also along the major dimension of the body. This refinement is required when the body is subjected to an EM field because the heat generation produced by the field is not uniformily distributed, as it is when the thermal load is caused by a conventional air environment. For this model the body is represented by 15 cylindrical segments and a sphere for the head, with each segment subdivided into four concentric layers consisting of a core layer, muscle layer, fat layer, and skin layer. As shown in Fig. 8, the neck, hands, and feet are approximated as single cylindrical segments, while the arms and legs are divided into four cylindrical segments and the trunk divided into three segments. The radius and length of each of these cylindrical segments are based on dimensions for a standard man [11]. Calculations of heat capacitance, thermal conductance, and density are based on the type of tissue, the surface area, and volume of each segment and layer. With this arrangement, the local temperature can be calculated at 100 positions throughout the body (the total number is actually 101 because the temperature of the central blood pool is also calculated).

The calculation of the temperature distribution in the above model is accomplished by a finite element solution of the well-known transient heat conduction equation in which internal heat generation is due to metabolism and absorption of EM energy. Internal dissipation is due to convective exchange with the cardiovacsular system, convective heat transfer in the lungs, and a combined convective and radiant exchange with the surrounding environment at the surface of the skin. The thermoregulatory mechanisms of vasodilation (increased blood flow) and sweating are called upon when the body's core temperature

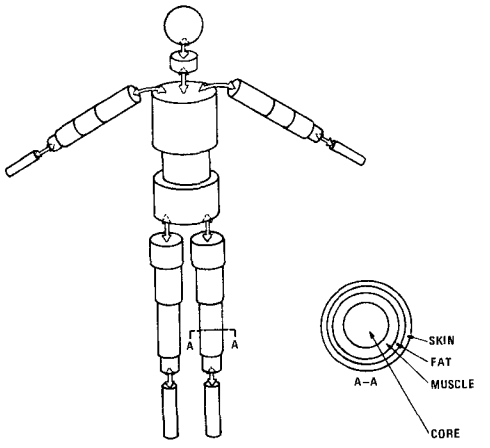

Fig. 8. The cylindrical model of man used for heat transfer calculations.

rises above the set point. The thermal balance equation simulating the response is, therefore, expressed as

$$\rho c(\partial T/\partial t) = \nabla(k \nabla T) + (1/V) \cdot (Q_{EM} + Q_M - Q_S - Q_B - Q_R) \quad (4)$$

where

Q_{EM}	EM power deposition;
Q_M	metabolic heat generation;
Q_S	evaporative heat dissipation in the skin;
Q_B	convective heat dissipation by the blood;
Q_R	respiratory heat loss in the lungs;
ρ	tissue density;
c	tissue specific heat;
T	local tissue temperature;
t	exposure time; and
V	tissue volume.

As convective heat transfer by blood flow plays a critical role in thermoregulation, it is necessary to increase blood flow to selected tissues in response to local temperature increases. While it is believed that all tissues respond to local temperatures in excess of 39°C by increasing blood flow, there is not enough physiological data available in the literature to include this response for all tissues in the body. Therefore, the model sets blood flow rates to all tissues, except the muscle and skin, at the basal values [10]. The skin blood flow rate is controlled by vasodilation and is a function of the temperature difference between the local skin temperature and the skin set-point temperature, as well as the difference between the hypothalamic temperature and its set-point temperature. Muscle blood flow is increased only when the body is performing work which requires oxygen in excess of basal levels.

Sweating is another very important thermoregulatory mechanism, and several mathematical models have been proposed to calculate heat lost by sweating [12]. All are empirical in nature and they attempt to best fit experimental data for a variety of conditions such as for a sedentary subject or for various levels of exercise. As with the blood flow rate, the term which simulates sweating is a function of the temperature difference between local skin temperature and the skin set-point temperature and the difference between the hypothalamic temperature and its set-point temperature.

As a physical basis for the skin blood flow and sweating to be controlled by both the skin and hypothalamus temperature difference, two important mechanisms must be recognized. First, it is known from experiments on animals that the hypothalamus is sensitive to temperature, and it acts as an internal "thermostat"; when it is warmed heat dissipating actions (sweating and dilation of the peripheral blood vessels) are initiated. A second mechanism must also exist because it is well known that the hypothalamus does not provide all the feed-back information to monitor the thermal state of the body. For example, if one enters a hot environment, sweating occurs before the hypothalamus experiences any temperature rise. The body takes corrective action long before there is any internal temperature rise. This could occur only if there exist peripheral temperature sensors on the skin of the body which provide the body's "thermostat" (hypothalamus) with information about rapid changes in the external thermal condition.

Numerical results will now be presented for both of the previously discussed situations; i.e., a human subject in close proximity to a $\lambda/4$ monopole and a $\lambda/2$ dipole. The normalized EM absorption conditions (input power to the antenna of 1 W) of Fig. 5 and 7 are converted to other power density levels by multiplying the normalized values by the new antenna input power values, which are specified according to

$$P_{in} = V_{rms}^2 G \quad (5)$$

where

V_{rms}	the rms voltage across the antenna's input terminals; and
G	the antenna's input conductance.

Antenna input power levels ranging from 1 to 1000 W are considered. The method whereby the absorbed power densities, as calculated by the EM model, are input to the thermal model has been described elsewhere [5].

A. Thermal Response Produced by the $\lambda/4$ Monopole

Fig. 9 shows selected core temperature increases versus antenna input power levels for steady-state thermal conditions. Attention has been paid to the core temperatures of the ankle and knee, as the leg is the most likely candidate for a hot spot because the EM model indicated high levels of absorbed power density there (see Fig. 5). Other temperatures considered are the temperature of the neck, hypothalamus, rectum, central blood pool, and the average body temperature (T_{Body}). The average or mean body temperature is obtained by averaging all the segment temperatures weighted by their thermal capacitance. Note the dramatic increase of both the ankle and knee temperatures relative

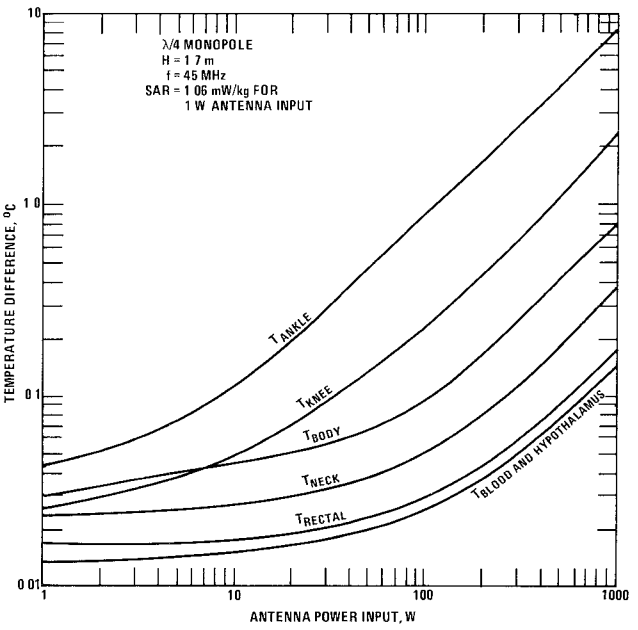

Fig. 9. Selected steady-state temperature increases produced by the λ/4 monopole antenna as a function of input power to the antenna.

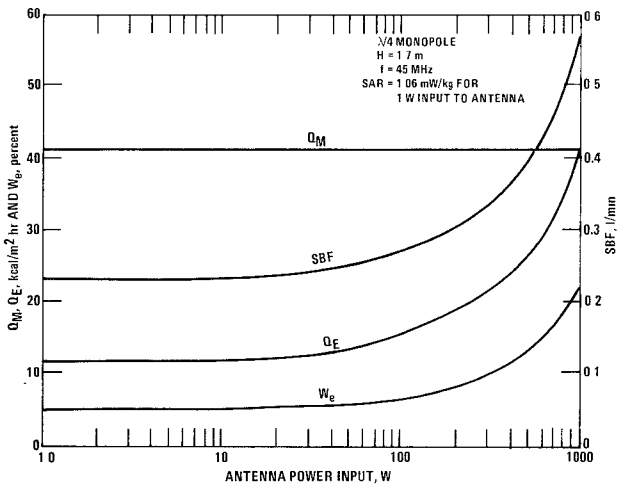

Fig. 10. Selected steady-state thermoregulatory responses produced by the λ/4 monopole antenna as a function of input power to the antenna.

to the other temperatures as the input power to the antenna is made larger. Fig. 10 contains the corresponding thermoregulatory responses of total skin blood flow (SBF), total evaporative heat loss (Q_E), the percentage of the skin surface covered with perspiration (W_E), the net rate of heat storage for the whole body (S), and the metabolic rate (Q_M). The total SBF is calculated by summing the blood flows associated with each skin segment, while the total evaporative heat loss and the net rate of heat storage are obtained by summing the evaporative heat loss and net heat flow, respectively, over all the segments. Heat flow, evaporative heat loss, and the metabolic rate are plotted in terms of Kcal/m^2·h, as obtained by dividing them by the total body surface area. They can be converted into watts by multiplying by 2.15. Based on both of these sets of curves, it is clear that a significant thermal response occurs only when the input power to the antenna is increased

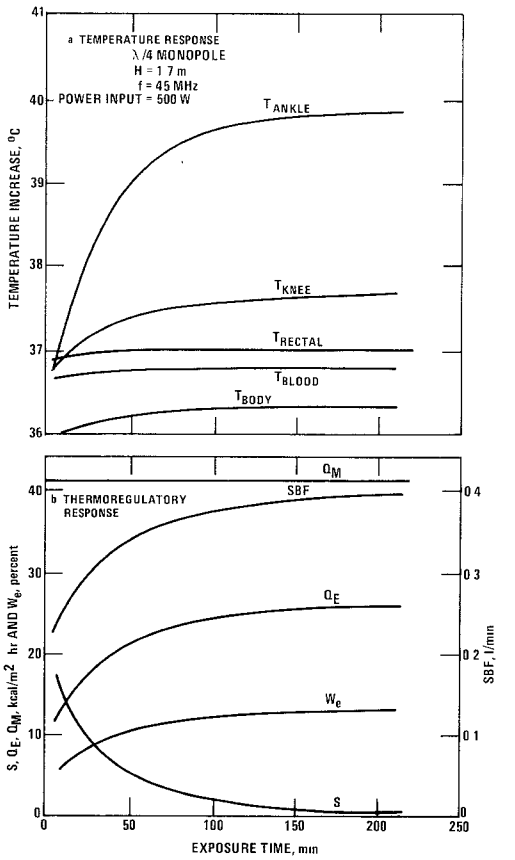

Fig. 11. Selected temperature and thermoregulatory responses produced by the λ/4 monopole antenna as a function of exposure time.

above around 50 W. Although there is a hot spot (a temperature of 41.6°C) in the leg when input power levels to the antenna are raised to 1000 W, the increased thermoregulatory responses of sweating and vasodilation are able to keep the average body and rectal temperature increases small.

In Fig. 11, selected temperatures and thermoregulatory responses are plotted versus exposure time when the input power to the antenna is 500 W. As can be seen, there is an instantaneous response of the body to the EM thermal load, but it takes around 90 min to reach thermal steady-state conditions. As was stated above, the ankle temperature is significantly elevated over the other temperatures, and a hot spot temperature of around 40°C is reached. This illustrates, and it should be emphasized, the fallacy of considering only rectal or average body temperature as an indicator of acute temperature rise. While the effect of blood circulation tends to lessen the magnitude of hot spots, it cannot remove them completely. In other words, hot spots will exist at locations predicted solely on the basis of the EM model, but their severity is reduced when blood flow and other thermoregulatory mechanisms are considered.

B. Thermal Response Produced by the λ/2 Dipole

Figs. 12–14 show the thermal response of a human when a λ/2 dipole, operated at 200 MHz, is placed very close (10 cm) to the head. All the quantities in these figures are

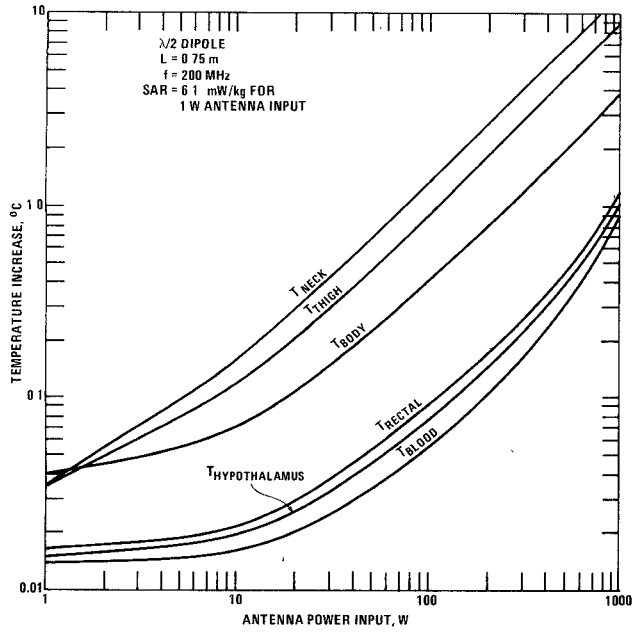

Fig. 12. Selected steady-state temperature increases produced by the λ/2 dipole antenna as a function of input power to the antenna.

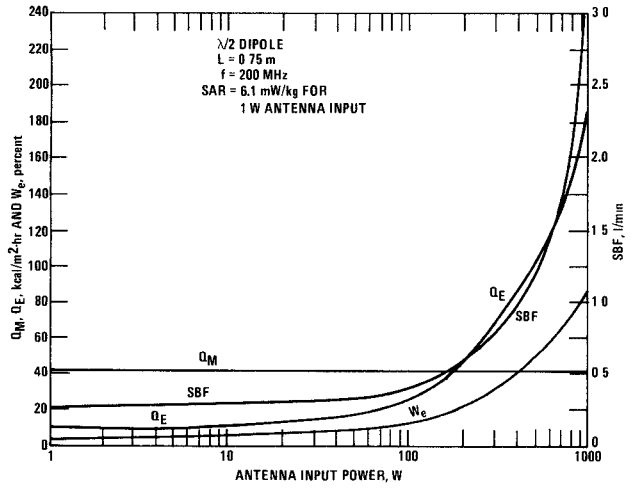

Fig. 13. Selected steady-state thermoregulatory responses produced by the λ/2 dipole antenna as a function of input power to the antenna.

the same as the previous case except the thigh core temperature is considered instead of the ankle or knee temperatures. Note that for this situation the location of the hot spot is in the neck. This location is to be expected as the logical candidate for a hot spot because the EM absorption model (see Fig. 7) predicted larger absorbed power densities there. Another important point is that the average whole body SAR is around six times greater than the previous case, consequently the body begins to thermally respond to the external fields at somewhat lower antenna input power levels.

C. Comparison with Plane-Wave Fields

These results can also be compared to plane-wave field heating patterns [5]. As the current U.S. safety standard is specified in terms of milliwatts per square centimeter, it is common for researchers to convert near-zone fields into an

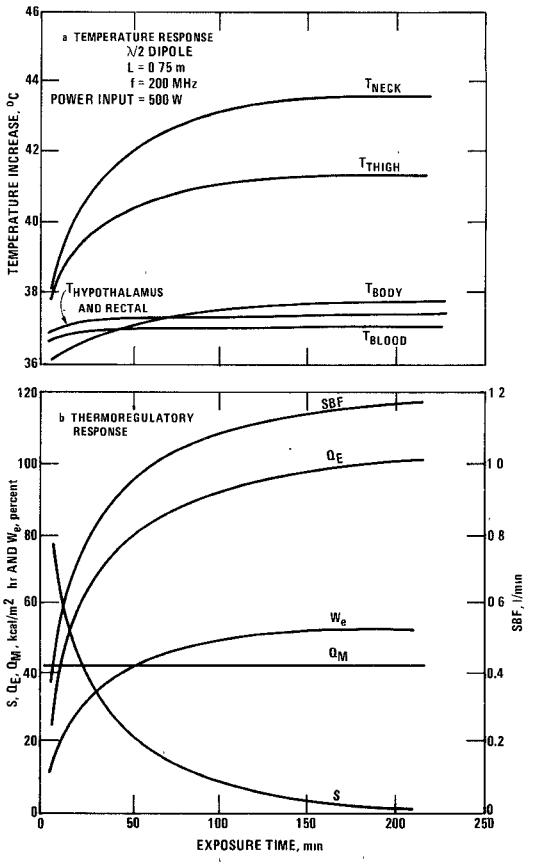

Fig. 14. Selected temperature and thermoregulatory responses produced by the λ/2 dipole antenna as a function of exposure time.

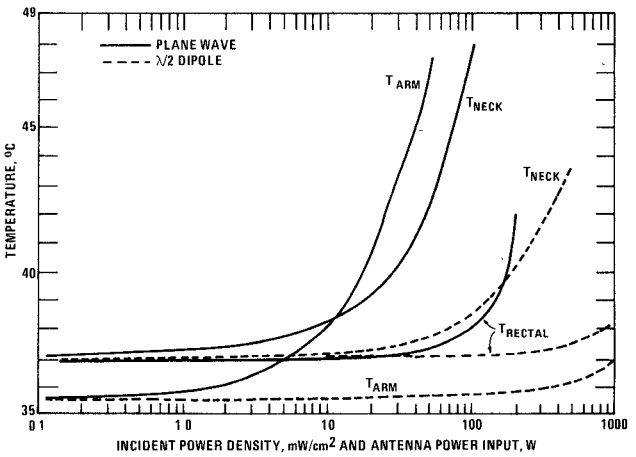

Fig. 15. A comparison of the heating effects of a 200-MHz plane wave with that of a λ/2 dipole operating at 200 MHz.

"equivalent power density" via

$$P = \frac{|E|^2_{\text{rms}}}{377}. \tag{6}$$

This is, of course, not correct because (6) is valid only for plane-wave fields.

The only legitimate method whereby near-zone thermal loading effects can be compared with plane-wave effects is through the resulting temperature distributions for both field types. For example, Fig. 15 compares temperatures at selected locations for a plane-wave field at 200 MHz with a

$\lambda/2$ dipole operating at 200 MHz. The plane wave is propagating from the front to the back of the body with its electric field oriented parallel to the body's major length. Fig. 15 plots the temperature increase versus incident power density for a plane-wave field as well as the input antenna power for the $\lambda/2$ dipole. The figure compares the rectal temperature and also the temperatures at peak temperature locations (lower humerus for the plane wave and the neck for the $\lambda/2$ dipole). Based on this comparison, it is clear that if the dipole near-zone fields were converted to plane-wave equivalent power density values, then the thermal loading effects of the dipole fields would be vastly overstated. In addition, the temperature distributions are greatly different; a hot spot exists in the arm for the plane-wave case, while for the $\lambda/2$ dipole a hot spot occurs in the neck.

IV. Discussion and Conclusions

The numerical simulation of the body's thermal response to antenna near-zone fields has been calculated. Two antenna-body configurations were considered. As might be expected, the heating patterns produced by the two antennas were different. The $\lambda/4$ monopole tended to produce elevated temperatures in the lower part of the legs, while the $\lambda/2$ dipole generated higher temperatures in the neck and upper torso. The $\lambda/2$ dipole was operated at 200 MHz, which is fairly close to the predicted head resonance frequency of 375 MHz. Whole body resonance for a human located over a ground plane was simulated by the $\lambda/4$ monopole operating at 45 MHz.

It was found that at least 50 W of input power are required before the body experienced any significant thermal effect from the near-zone antenna fields. Because worst case conditions were simulated (whole-body resonance and near-head resonance for the object and also resonant conditions for the antennas), these results imply that a person holding a 2-W transmitter or standing near a CB antenna operating at 27 MHz, should not experience any acute thermal loading from the antenna fields. It should be pointed out, however, that CB type antennas can also be loaded (top and base) to increase radiation efficiency. This tends to also increase near-zone fields [13], and consequently these antenna conditions should also be simulated.

On the other hand, the model indicates that high power communication antennas operating in amateur, land, and maritime mobile bands, etc., with input power levels ranging from 100 to 1000 W will produce near-zone fields that can probably cause thermal loading in a human situated close to the antenna. Separation distances which minimize thermal loading can be estimated by a consideration of Fig. 3. When the object is located 20 cm from the antenna, near-zone field strengths are around 35 V/m for 1 W of input power. If the antenna input power is increased to 1000 W, then the field strength is approximately equal to $\sqrt{1000} \cdot 35$ or 1107 V/m. It has been shown that 10 W of input power do not significantly elevate body temperatures (see Fig. 8). This input power level corresponds to $\sqrt{10} \cdot 35$ or 111-V/m fields. Thus, the fields produced by the 1000-W transmitter should be decreased by a factor of 10 (or 1107/111). From Fig. 3, this means that the body has to be placed around 2.5 m from the 1000-W source in order to minimize thermal loading effects.

It should also be emphasized, and it was pointed out earlier, that it is believed most tissues respond to local temperatures in excess of 39 or 40°C by increasing blood flow. This increased blood flow response was not included in this model because there does not appear to be enough quantitative information available in the literature to accurately model this response for all the compartments in the model. Therefore, a conservative approach was taken by setting blood flow rates to all tissues, except the skin, at the basal levels. Skin blood flow rate was controlled by vasodilation. This would imply that for the calculations reported here, the model tends to overestimate the magnitude of the ankle, thigh, and neck hot spots produced by antennas with input power levels greater than around 200 of 300 W.

Another problem is that the absorbed power density distribution, as calculated by the EM model, exhibits considerable spatial variation over the body. Much of this variation was averaged out when it was input to the thermal model. Thus the thermal model needs to be improved by increasing the number of cells or compartments. This implies that the current two-dimensional thermal model, which includes heat transfer in both the radial and axial directions, needs to also to take into account heat flow on the azimuthal direction. While these extensions are numerically straightfoward, problems may arise in computer storage requirements and in computaional time (cost) to generate the heating patterns.

Finally, even though the thermal model yields results which compare well with experimental measurements of a human subject placed in a room at a controlled temperature and relative humidity [14], it is certainly open to question whether good agreement between measured and calculated results would likewise be obtained when the thermal load is caused by an EM field. To that end, our laboratory is currently building the necessary anechoic chamber for making thermal physiological measurements on a monkey exposed to an EM field at or near the animal's whole body resonant frequency. Because monkeys have thermoregulatory systems that are similar to man, they are a good thermal subject and consequently verification of the numerical model based on data taken on monkeys is tantamount to verification in human subjects.

References

[1] R. A. Tell and F. Harlen, "A review of selected biological effects and dosimetric data useful for development of radiofrequency safety standards for human exposure," *J. Microwave Power*, vol. 14, no. 4, pp. 405–424, Apr. 1979.

[2] E. J. Lerner, "RF radiation: biological effects," *IEEE Spectrum*, pp. 51–59, Dec 1980.

[3] K. Karimullah, K. M. Chen, and D. P. Nyquist, "Electromagnetic coupling between a thin-wire antenna and a neighboring biological body: theory and experiment," *IEEE Trans. Microwave Theory Tech.*, vol. MTT-28, pp. 1218–1225, Nov. 1980.

[4] I. Chatterjee, M. J. Hagmann, and O. P. Gandhi, "Electromagnetic energy deposition in an inhomogeneous block model of man for near-field irradiation conditions," *IEEE Trans. Microwave Theory Tech.*, vol. MTT-28, pp. 1452–1459, Feb. 1980.

[5] R. J. Spiegel, D. M. Deffenbaugh, J. E. Mann, "A thermal model of the human body exposed to an electromagnetic field," *Bioelectromagnetics*, vol. 1, no. 3, pp. 253–270, 1980.

[6] C. H. Durney, C. C. Johnson, P. W. Barber, H. Massondi, M. F. Iskander, J. L. Lords, D. K. Ryser, S. J. Allen, and J. C. Mitchell, "Radiofrequency radiation dosimetry handbook (second edition)," USAF School of Aerospace Medicine, Brooks Air Force Base, TX, Tech. Rep. SAM-RT-78-22, May 1978.

[7] M. J. Hagmann, "Head resonance: numerical solutions and experimental results," *IEEE Trans. Microwave Theory Tech.*, vol. MTT-27, pp. 809–813, Sept. 1979.

[8] K. Karimullah, "Theoretical and experimental study of the proximity effects of thin-wire antenna in presence of biological bodies," Ph.D. dissertation, Michigan State University, East Lansing, MI, 1979.

[9] M. J. Hagmann, O. P. Gandhi, and C. H. Durney, "Numerical calculation of electromagnetic energy deposition for a realistic model of man," *IEEE Trans. on Microwave Theory Tech.*, vol. MTT-27, pp. 804–809, Sept. 1979.

[10] J. A. J. Stolwijk, "A mathematical model of physiological temperature regulation in man," NTIS, Springfield, VA, NASA CR-1855/NTIS N71-33401, Aug. 1971.

[11] N. Diffrient, A. R. Tilley, and J. C. Bardagjy, *Humanscale 1/2/3*. Cambridge, MA: M.I.T. Press, 1974.

[12] A. F. Emery, R. E. Short, A. W. Guy, and K. K. Kraning, "The numerical thermal simulation of the human body when undergoing exercise or nonionizing electromagnetic irradiation," *Trans. Amer. Soc. Mech. Eng.*, pp. 284–291, May 1976.

[13] P. S. Ruggera, "Measurements of electromagnetic fields in the close proximity of CB antennas," HEW Publication (FDA) 79-8080, Jan. 1979.

[14] J. D. Hardy and J. A. J. Stolwijk, "Partitional calorimetric studies of man during exposures to thermal transients," *J. Appl. Physiol.*, vol. 21, no. 6, pp. 1799–1806, Nov. 1966.

Ronald J. Spiegel (M'73), was born in Cleveland, OH, on May 31, 1942. He received the B.E.E. degree in 1964 from the Georgia Institute of Technology, the M.S.E.E. degree in 1966 from the University of Arkansas, and the Ph.D. degree in electrical engineering in 1970 from the University of Arizona.

From 1971 to 1972 he was a Post Doctoral Fellow in biomedical engineering at Duke University. In 1973 he joined the Boeing Aerospace Company, Seattle, WA as a research engineer engaged in studies of nuclear electromagnetic pulse (EMP) effects on aeronautical electrical systems. From 1974 to 1976 he was with IIT Research Institute, Chicago, IL, involved in research in bioelectromagnetics and extra low frequency (ELF) coupling, interference mitigation, and environmental studes associated with the Navy Seafarer antenna. From 1976 to 1980 he was with Southwest Research Institute, San Antonio, TX, performing research in a variety of areas such as EMC, electrostatics, bioelectromagnetics, and electromagnetic geophysical exploration. He is presently with the U.S. Environmental Protection Agency, Research Triangle Park, NC, working in the area of microwave field interaction with biological media and dosimetric methods.

Dr. Spiegel is a member of the Eta Kappa Nu, Sigma Xi, Bioelectromagnetics Society, and is a Registered Professional Engineer.